Phase Compensation Strategies for Modulated-Demodulated Control With Application to Pulsed Jet Injection

Cory Hendrickson

Robert T. M'Closkey
e-mail: rtm@seas.ucla.edu

Department of Mechanical and Aerospace
Engineering,
University of California, Los Angeles,
Los Angeles, CA 90095

Modulated-demodulated control is an effective method for asymptotic disturbance rejection and reference tracking of periodic signals, however, conventional static phase compensation often limits the loop gain in order to avoid sensitivity function peaking in a neighborhood of the frequencies targeted for rejection or tracking. This paper introduces dynamic phase compensation for modulated-demodulated control which improves disturbance rejection characteristics by inverting the plant phase in a neighborhood of the control frequency. Dynamic phase compensation is implemented at baseband which enables the use of low-bandwidth compensators to invert high frequency dynamics. Both static and dynamic phase compensation methods are used to demonstrate a novel application of repetitive control for pulsed jet injection. In this application pulsing an injectant has been shown to produce advantageous effects such as increased mixing in many energy generation and aerospace systems. The sharpness of the pulse can have a large impact on the effectiveness of control. Modulated-demodulated control is used to maximize the sharpness of a pulsed jet of air using active forcing by tracking a square wave in the jet's temporal velocity profile. [DOI: 10.1115/1.4004768]

Keywords: modulated and demodulated systems, repetitive control, flow control, periodic reference tracking

1 Introduction

The disturbance rejection and reference tracking problem of periodic signals is encountered in many engineering systems. As such, there has been extensive research on repetitive control documented in the literature over a wide range of applications such as industrial machinery [1], AC power supplies [2,3], computer disk drives [4–6], and helicopter blade control [7,8]. All types of repetitive control are united in their basis, directly or indirectly, by Francis and Wonham's internal model principle (IMP) which requires a model of the disturbance or reference to be included in the feedback loop for perfect rejection or tracking [9]. One method of repetitive control is modulated-demodulated control, sometimes referred to as adaptive feedforward control or adaptive feedforward cancellation [10,11]. This approach shifts the spectrum of "high" frequency oscillations down to baseband which includes DC, operates at baseband, then shifts the baseband spectrum back to high frequency. Essentially, the plant output in a neighborhood of the frequency to be controlled is estimated by demodulation and low-pass filtering, then manipulated to form an input based on known plant dynamics which will cancel the estimated disturbance or track a reference signal.

Modulated-demodulated control is based indirectly on the IMP as shown in Ref. [12], where Bodson *et al.* prove the equivalence of a simple modulated-demodulated controller and a controller based directly on the IMP, the basis of the latter being a harmonic oscillator with transfer function

$$C_{imp}(s) = \frac{ks}{s^2 + \omega^2}$$

Both methods can be extended to reject/track multiple sinusoidal frequencies by placing copies of either controller in parallel.

Alternatively, the time delay repetitive controller, which has transfer function based on a time delay, L

$$C_{td}(s) = \frac{e^{-Ls}}{1 - e^{-Ls}}$$

controls at multiple frequencies but is restricted to control harmonics of the fundamental frequency $1/L$. The modulated-demodulated controller and IMP controller both offer selective placement of poles; however, modulated-demodulated control can be more advantageous in implementation because low-bandwidth compensators are used to control high frequency oscillations.

Most modulated-demodulated control studies to date have focused on disturbance rejection such as in Refs. [13] and [14] where a modulated-demodulated controller is used for vibration damping in flexible structures. Their design relies upon the fact that vibration occurs at distinct modes dictated by the resonances of the structure. The modulation frequencies of the controller are placed at the resonances to provide damping. Analysis shows a linear time-invariant (LTI) transfer function for this controller can be derived from two different perspectives, either the high frequency "control band" or the low frequency "baseband." The control band analysis provides information on performance while the baseband analysis provides greater insight into the controller design.

The present paper expands upon the insight gained from the baseband analysis of Ref. [14] and presents an improved method of phase compensation for modulated-demodulated control. Replacing conventional static phase compensation with dynamic phase compensation improves disturbance rejection nearby the specified rejection or tracking frequency. Additionally, static phase and dynamic phase modulated-demodulated controllers are used to demonstrate a novel application of repetitive control for pulsed jet injection. Actively pulsing a jet can favorably influence many aspects of a flowfield such as the spread and mixing of the jet into its surroundings. It is hypothesized these parameters will be maximized with the formation of strong, well spaced vortex rings at the jet exit. Periodic square wave forcing is believed to be

the most effective way to accomplish this but challenges are presented in forming square waves due to nonlinear dynamics identified in the actuation system. Repetitive control is necessary to shape the jet's measured temporal velocity waveform to track, as closely as possible, a square wave.

2 Controller Architecture

The present strategy applies to single input, single output systems. A parallel set of individual control loops, each designed to operate in a narrow band around a single frequency, are summed together to achieve the overall goal of rejecting a disturbance and its harmonics or tracking a periodic reference waveform. The operating frequencies are positioned at the fundamental frequency, denoted ω_f, of the periodic disturbance or reference and a specified number of its harmonics. Thus, the ideal measured waveform will cancel the disturbance or match the Fourier series approximation of the periodic reference truncated at the number of harmonics tracked.

2.1 Control at a Single Frequency. Each individual control loop demodulates the measurement y to shift the spectrum of y in the neighborhood of the demodulation frequency down to a baseband, operates at the baseband near DC, and then modulates the signal back up to "high" frequency. This process is detailed in Fig. 1 for control at a single frequency, denoted ω_o. The output of the plant, P, is split into two branches by demodulation with 2 $\cos(\omega_o t)$ and 2 $\sin(\omega_o t)$ to produce y_c and y_s in Fig. 1. These signals are then low-pass filtered by H_{LP} (unity gain at DC) and compared to the constants C_1 and C_2 which represent the Fourier series coefficients of the desired harmonic signal

$$C_1 \cos(\omega_o t) + C_2 \sin(\omega_o t) \tag{1}$$

The error signals are integrated and then compensated to implement an approximate phase inversion of P which produces favorable stability and sensitivity characteristics of the closed-loop system. The method of phase compensation distinguishes the control strategies presented in this paper from one another. Phase compensation is accomplished statically or dynamically (as shown in Fig. 1) depending on the characteristics of P. Following this stage, the signals are modulated back to the control band by $\cos(\omega_o t)$ and $\sin(\omega_o t)$, summed, and scaled by K to produce the control effort u. If control at multiple frequencies is desired, the architecture is repeated for each frequency and the output of each control loop is summed.

Under periodic reference tracking conditions the output has its energy concentrated in narrow bands around the harmonics of the fundamental forcing frequency. This is similar to the narrow-band resonant structure sensor response used for feedback in the modulated-demodulated controller of Ref. [14]. The response of y in a neighborhood of ω_o is captured by the signals y_1 and y_2, i.e.

$$y(t) = y_1(t) \cos(\omega_o t) + y_2(t) \sin(\omega_o t)$$

in a neighborhood of ω_o because the low-pass filters, denoted H_{LP} in Fig. 1, band-limit y_1 and y_2 [15]. If the corner frequency of H_{LP} is denoted ω_c, then y_1 and y_2 can be used to reconstruct y in the $[\omega_o - \omega_c, \omega_o + \omega_c]$ band. When a periodic waveform is tracked, multiple copies of Fig. 1 are summed with ω_o set to the fundamental frequency of the periodic waveform and a select number of its harmonics. In this case, the corner frequencies associated with each harmonic is limited to be $\omega_c < \omega_{f/2}$ so controllers at adjacent harmonics do not interact.

The reference signal in this setup is injected into the baseband via constants C_1 and C_2. These specify the plant output in the form of Eq. (1). When C_1 and C_2 are set to 0, this type of controller is often given the name adaptive feedforward cancellation due to its effectiveness at canceling periodic output disturbances. However, for the purposes of reference tracking, C_1 and C_2 are set to the real and imaginary parts of the Fourier series coefficient at frequency ω_o of a periodic reference waveform.

Phase compensation in modulated-demodulated control is needed to invert the phase of P to reduce the classical sensitivity function of the closed-loop system in a neighborhood of ω_o. This has typically been accomplished using a phase advance parameter given to the demodulators to adjust the controller's phase by a constant angle. In this study, we use an alternative implementation for phase compensation which employs either a stage of constant gains or a stage of compensators, respectively, to create a static or dynamic phase characteristic in a neighborhood of ω_o. The static phase compensation controller uses constant gains, denoted R and I, in place of the dynamic compensators H_d and H_x of Fig. 1. The static phase approach is an equivalent implementation of the phase advance parameter [16]. The phase angle of the rotation, denoted ϕ, is defined by gains R and I through the rotation matrix

$$Q = \begin{bmatrix} R & I \\ -I & R \end{bmatrix}$$

The phase rotation is set to cancel the phase delay of the plant frequency response at ω_o to maximize phase margin of the system [6]. The static phase compensation gains are defined as follows

$$R = \frac{R_p}{\sqrt{R_p^2 + I_p^2}} \quad \text{and} \quad I = \frac{I_p}{\sqrt{R_p^2 + I_p^2}} \tag{2}$$

where

$$P(j\omega_o) = R_p + jI_p \tag{3}$$

The structure of this implementation is advantageous for our purposes as the extension from static to dynamic phase compensation is easily accomplished by replacing the static phase compensation
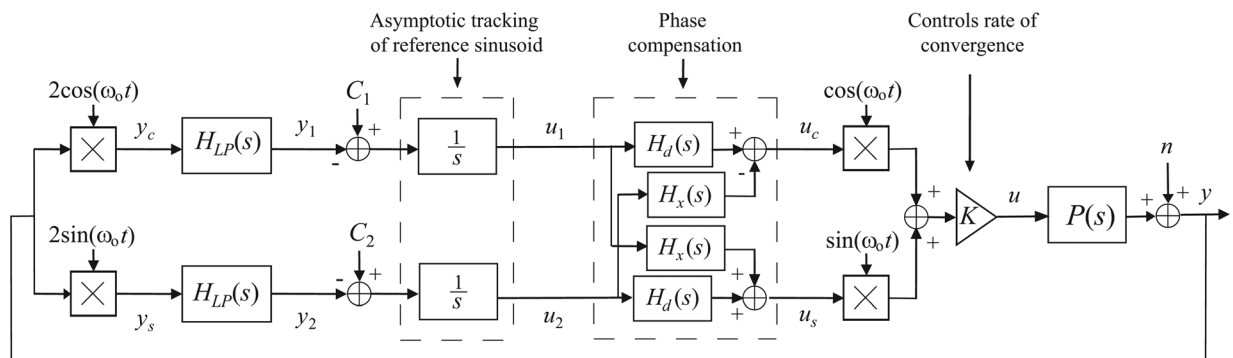

Fig. 1 The "Dynamic phase" modulated-demodulated controller for asymptotic reference tracking of a single sinusoid at frequency ω_o

gains with dynamic compensators. Dynamic phase compensation reduces the sensitivity function of the closed-loop system by inverting the plant phase in a neighborhood of ω_o. This method is most useful when P has rapidly changing phase nearby ω_o. Expression for H_d and H_x are developed in Sec. 3.

3 Controller Analysis

The modulated-demodulated system presented above is split into two distinct bands, the high frequency "control band" and the low frequency baseband. As in Ref. [14], it is natural and useful to analyze the system from both perspectives. An exact LTI transfer

function from y to u can be derived for the controller from the control band perspective, however, from the baseband perspective, the controller can be represented by a two input, two output (TITO) baseband controller, from $[y_1\ y_2]^T$ to $[u_1\ u_2]^T$ and a TITO compensated plant.

3.1 Control Band Analysis. The fact the controller can be represented as an LTI system is not straightforward. Using Laplace transforms with an arbitrary phase γ given to the modulating and demodulating signals, $\cos(\omega_o t + \gamma)$ and $\sin(\omega_o t + \gamma)$, it can be shown the transfer function for control at a single frequency using dynamic phase compensation is given by

$$C_d(s) = K\left[\frac{H_{LP}(s - j\omega_o)(H_d(s - j\omega_o) - jH_x(s - j\omega_o))}{s - j\omega_o} + \frac{H_{LP}(s + j\omega_o)(H_d(s + j\omega_o) + jH_x(s + j\omega_o))}{s + j\omega_o}\right] \tag{4}$$

This expression is independent of γ and, thus, represents a time-invariant compensator. Using integrators as the baseband controller produces the required poles at $\pm j\omega_o$ for perfect steady state tracking of periodic references as dictated by the internal model principle. The poles of H_{LP} have also been shifted to $\pm j\omega_o$, creating a bandpass filter positioned around ω_o with corner frequencies at $\omega_o \pm \omega_c$. With static phase compensation the transfer function simplifies to

$$C_s(s) = K\left[\frac{H_{LP}(s - j\omega_o)}{s - j\omega_o}(R - jI) + \frac{H_{LP}(s + j\omega_o)}{s + j\omega_o}(R + jI)\right] \tag{5}$$

The subscripts d and s refer to the dynamic phase controller and static phase controller, respectively. It is worth noting that without H_{LP} and phase compensation ($R = 1$ and $I = 0$), the modulated-demodulated controller is equivalent to the internal model principle controller, C_{imp}, which was shown in Ref. [12].

The loop gain $L = PC$ closely resembles, for sufficiently small gain K, the force-to-velocity harmonic oscillator transfer function in a neighborhood of ω_0

$$L(s) \approx \frac{2Ks}{s^2 + \omega_o^2}|P(j\omega_o)| \tag{6}$$

The factor of 2 is needed to be consistent with the block diagram of Fig. 1. This expression is used to approximate the rate of convergence at each control frequency for both static and dynamic phase compensators. Dynamic phase compensation permits the use of larger values of K for which Eq. (6) is still a reasonable approximation of L in a neighborhood of ω_o. When unity gain negative feedback is closed around Eq. (6), the closed-loop system has time constant $\tau = 1/K|P(j\omega_o)|$.

One of the advantages of modulated-demodulated control is the ability to independently specify the convergence rate at each frequency of control. For example, the individual loop gains can be set to be inversely proportional to the plant magnitude at ω_o to equate the convergence rates at all frequencies. More precisely, K can be chosen as

$$K = \frac{1}{\tau|P(j\omega_o)|} \tag{7}$$

in order to achieve the closed-loop time constant τ at all control frequencies. This choice is used for the application discussed in Sec. 4 where the magnitude of the plant frequency response decreases by almost 2 orders of magnitude within the actuation bandwidth.

3.2 Baseband Analysis. The motivation for development of dynamic phase compensation is best illustrated by analysis of the static phase controller from the baseband perspective. A static phase compensated plant, denoted G_s, is defined as the TITO system from $[u_1\ u_2]^T$ to $[y_1\ y_2]^T$ in Fig. 1 (the loops are broken between these signals and the $\frac{1}{s}$ compensators are removed). This is a linear, time-periodic system that can be approximated by an LTI system if

$$|H_{LP}(j\omega)| \approx 0 \text{ when } \omega > \omega_c \tag{8}$$

If Eq. (8) is valid, the 2×2 system of transfer functions for the static phase compensated plant is given by

$$G_s(s) = \begin{bmatrix} Y_{sd}(s) & Y_{sx}(s) \\ -Y_{sx}(s) & Y_{sd}(s) \end{bmatrix} \tag{9}$$

where

$$Y_{sd}(s) = K\frac{1}{2}[P(s - j\omega_o)(R + jI) + P(s + j\omega_o)(R - jI)]H_{LP}(s)$$

$$Y_{sx}(s) = K\frac{j}{2}[-P(s - j\omega_o)(R + jI) + P(s + j\omega_o)(R - jI)]H_{LP}(s)$$

At $s = 0$, $Y_{sx}(0) = 0$, provided Q exactly inverts the plant phase at ω_0. Additionally, $Y_{sd}(0) = 1$ provided both K and Q exactly invert the magnitude and phase of the plant at ω_o, therefore

$$G_s(0) = I_2$$

The two branches of the baseband are decoupled at DC. This effectively isolates control of the in-phase and quadrature terms of the demodulated signal. With a nondiagonal G_s, the in-phase and quadrature terms corrupt one another and reduce the phase margin of L_s. In general, only at $s = 0$ will G_s be diagonal even with $\phi = -\angle P(j\omega_o)$. It is likely any physical plant will have changing phase in the neighborhood of ω_o and, therefore, the controller will not exactly invert the plant phase except at ω_o. This has the potential to significantly degrade the performance of the controller due to peaking in the sensitivity function close to the control frequency. This can be avoided by reducing K at the expense of smaller bandwidth and slower convergence rate. Alternatively, dynamic phase compensation can improve the stability and sensitivity characteristics of the closed-loop system, without reducing K, by diagonalizing G_s over a range of s instead of only at $s = 0$. The dynamic phase compensated plant, denoted G_d, is
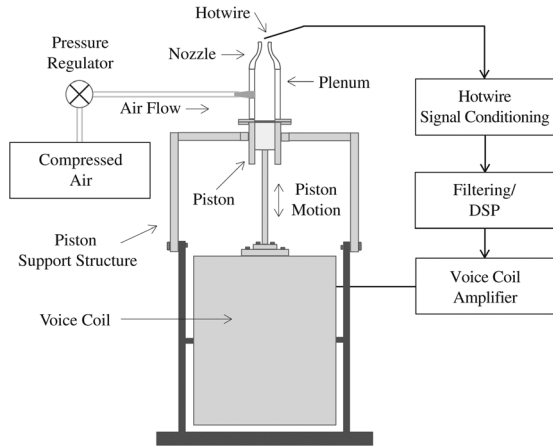
Fig. 2 Pulsed jet injection experimental setup. A piston, actuated by a modal shaker, is used to actively control the temporal velocity profile of a jet at the nozzle exit.

$$G_d(s) = \begin{bmatrix} Y_{dd}(s) & Y_{dx}(s) \\ -Y_{dx}(s) & Y_{dd}(s) \end{bmatrix} \quad (10)$$

where

$$Y_{dd}(s) = K\frac{1}{2}[P(s-j\omega_o)(H_d(s)+jH_x(s))+P(s+j\omega_o)$$
$$\times(H_d(s)-jH_x(s))]H_{LP}(s)]H_{LP}(s)$$

$$Y_{dx}(s) = K\frac{j}{2}[-P(s-j\omega_o)(H_d(s)+jH_x(s))+P(s+j\omega_o)$$
$$\times(H_d(s)-jH_x(s))]H_{LP}(s)$$

Setting

$$Y_{dd}(s) = 1 \text{ and } Y_{dx}(s) = 0$$

it can be shown the diagonal and off-diagonal compensators must take the form

$$H_d(s) = \frac{P(s-j\omega_o)+P(s+j\omega_o)}{2P(s-j\omega_o)P(s+j\omega_o)H_{LP}(s)} \quad (11)$$

$$H_x(s) = j\frac{P(s-j\omega_o)-P(s+j\omega_o)}{2P(s-j\omega_o)P(s+j\omega_o)H_{LP}(s)} \quad (12)$$

By setting $Y_{dd} = 1$, H_d and H_x invert both the magnitude and phase of P. Therefore, each loop gain is set equal to match the convergence rates at all frequencies. In practice, H_d and H_x are obtained by fitting stable filters to the graphs of (11) and (12) where P is given by empirical frequency response data.

3.3 Benefits of Controller Architecture In addition to independent manipulation of the convergence rate, modulated-demodulated control offers more flexibility than other repetitive control techniques because of decoupling between each individual rejection/tracking frequency of the controller. The frequency, gain, reference, and phase compensation parameters can be independently tuned within each frequency loop. Therefore, it is possible to target specific frequencies, even those which are not harmonics of the fundamental. It can be used to track a desired waveform as well as cancel periodic disturbances at unrelated frequencies.

When implemented digitally, the modulated-demodulated controller has an advantage over time delay repetitive controllers because the sampling rate does not have to be an integer multiple of the control frequency. Furthermore, this method of control is desirable because it only requires knowledge of the plant in a neighborhood of the fundamental and harmonics. In fact, identification of the relevant parameters can be done in the baseband "coordinates," i.e., Y_{dd} and Y_{dx} can be identified when $H_d = 1$ and $H_x = 0$.

4 Experimental Application to Pulsed Jet Injection

4.1 Experimental Setup The modulated-demodulated controllers developed in this study are used to demonstrate possible benefits of pulsed jet injection using the schematic shown in Fig. 2. The jet fluid, comprised of compressed air, is distributed into a plexiglass plenum via a four way injection. The flow is regulated to maintain an average jet velocity of 8 ms^{-1}. The velocity is measured using a hotwire anemometer placed at the exit of a contracting nozzle. Active forcing is applied using a lightweight
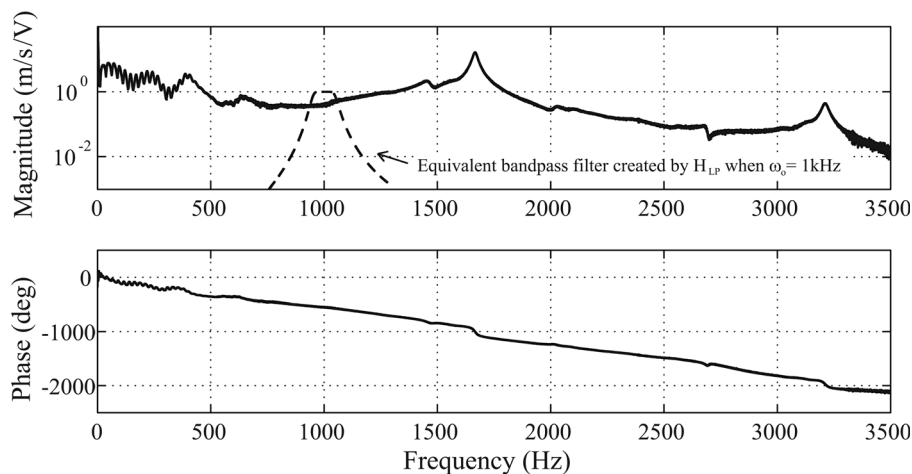

Fig. 3 Actuation system frequency response. The magnitude roll-off after the plenum mode at 1.7 kHz produces an actuator with an approximate bandwidth of 2 kHz. The dashed line represents the bandwidth for control around a single frequency with $\omega_c = 50$ Hz. The linear phase delay represents a significant transport lag which makes high-gain, wide bandwidth control impossible to achieve.

piston positioned beneath the injection point within the plenum, approximately 14 cm beneath the hotwire. The piston is actuated using a Ling LVS-100 modal shaker which moves with one degree of freedom, axially in line with the jet. The controllers are implemented using MATLAB's XPC Target application with a 25 kHz sampling rate. Anti-aliasing of the hotwire signal is accomplished using an 8-pole low-pass Chebyshev filter with a 10 kHz corner frequency.

4.2 System Identification. The piston actuation system was identified in a frequency band extending from 10 Hz to 5 kHz using a band-limited white noise input whose intensity is adjusted so that the RMS of the velocity perturbation is 0.2 ms^{-1}. As shown in Fig. 3, the frequency response rolls off after a mode at 1.7 kHz (due to a resonance of the plenum). Above approximately 2 kHz it becomes nearly impossible to influence the jet velocity. Such a limitation on the actuation system's bandwidth presents an obstacle when attempting to achieve a desired waveform, particularly a square wave. Due to the discontinuity in the waveform, the Fourier series coefficients of a square wave decay at a slow rate as a function of frequency especially when the duty cycle is small ($<20\%$). Thus, given the limited actuation bandwidth, only a limited number of harmonics of the fundamental forcing frequency can be used which produces a truncated version of an ideal square wave reference waveform. The truncated version of the square wave has oscillations in velocity near the discontinuity and a gradual transition from low-to-high or high-to-low velocity. The speed of the transition is dependent on the number of harmonics included in the truncation, with the greater number or harmonics leading to a faster transition. It is important to use as many harmonics as possible since a rapid transition is believed to produce strong vortex rings which improve the spread and penetration of the jet.
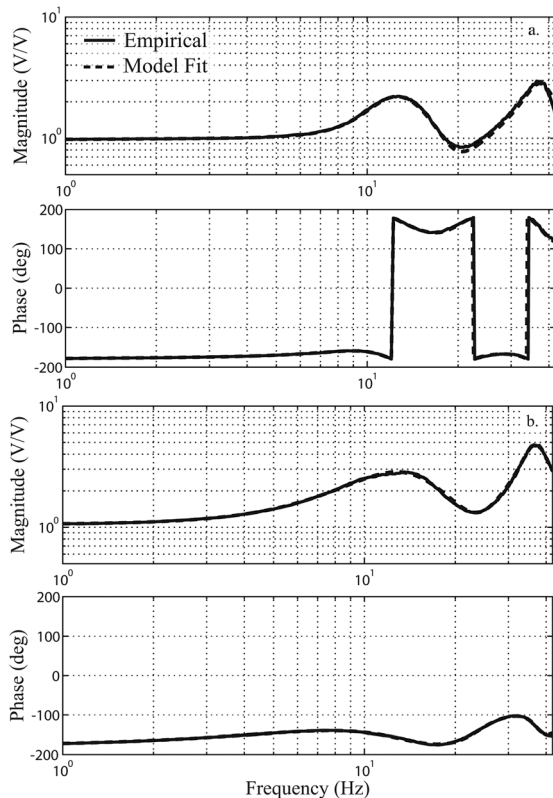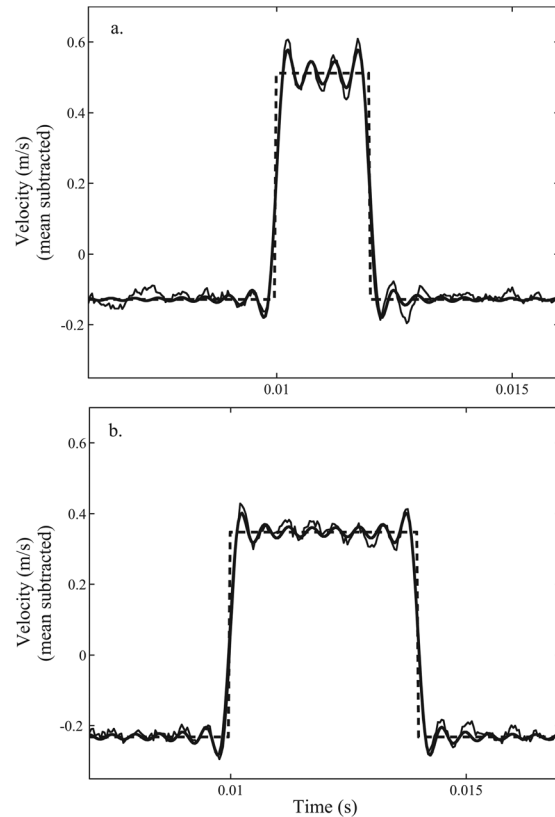

Fig. 5 Details of pulses produced with a repetition rate of 100 Hz and $\alpha = 20\%$ (case a), and $\alpha = 40\%$ (case b). One period of an ideal square wave (dashed line) is compared to the ideal square wave truncated at 20 sinusoids (thick solid line) and the empirical square wave (thin solid line).

In addition to the roll-off, the frequency response displays a large amount of delay over the frequency band of interest. One contribution to the delay is the transport lag created by the physical distance between the piston and hotwire. Such a large delay makes high-gain control impossible across the entire usable bandwidth of the actuator. Thus, instead of using a wideband approach,

Fig. 4 An example of dynamic phase compensators for plant phase inversion in a neighborhood around the control frequency ($\omega_o = 100$ Hz). Solid line—empirical, dashed line—model fit. (a) H_d and (b) H_x. The empirical data are fit up to 42 Hz using an eighth order and sixth order model for H_d and H_x, respectively.
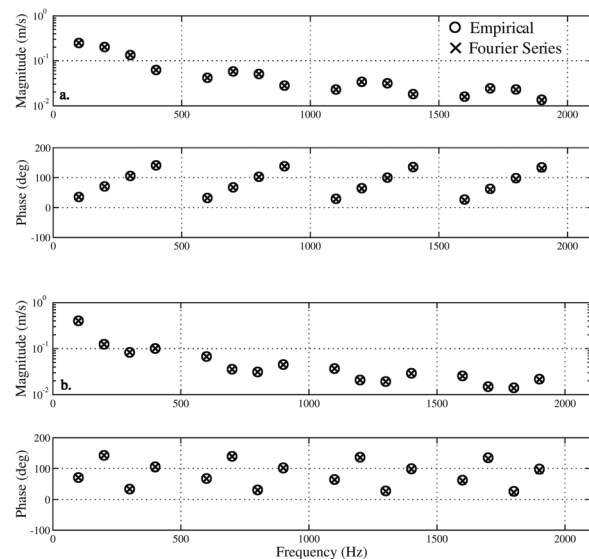

Fig. 6 Square wave spectrum (a) $\alpha = 20\%$ and (b) $\alpha = 40\%$. The empirical square wave spectrum at each forcing frequency (circles) is identical to the ideal square wave Fourier series (Xs).
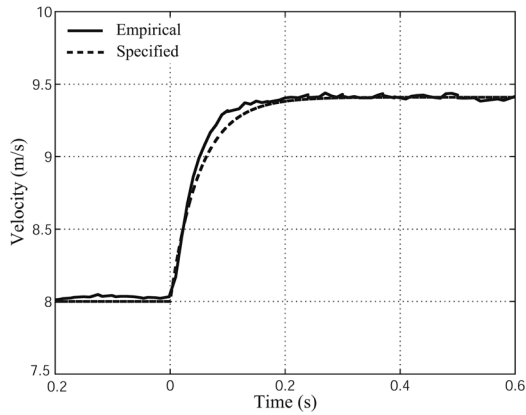
Journal of Dynamic Systems, Measurement, and Control

JANUARY 2012, Vol. 134 / **011024-5**

Fig. 7 Envelope of the response of a $\omega_o = 100$ Hz dynamic phase controller to a 1.4 ms^{-1} step input. The controller's gain is determined by a specified time constant of $\tau = 0.050$ s to be $K = 20/|P(j\omega_o)|$.

our control problem will be broken down into multiple narrow-band control problems using modulated-demodulated control with each frequency band positioned around the fundamental frequency and harmonics of the periodic reference waveform. The dashed line in Fig. 3 is representative of the bandwidth used for control at a single frequency using $\omega_c = 50$ Hz. Control over the entire usable bandwidth of the actuation system is achieved by summing the control effort from similar narrow bands.

Another notable feature of the plant's frequency response are the "ripples" at frequencies below 400 Hz, which are caused by dynamics associated with the injection tubing. In fact, the rapidly varying plant phase in this frequency range motivates the development of dynamic phase compensation because of the quantitative improvement that it provides over static phase compensation in terms of the system's closed-loop sensitivity characteristics.

4.3 Controller Implementation. Implementation of the static phase compensation controller only requires knowledge of the plant at ω_o. For a single- or multi-frequency controller this is rapidly accomplished on a sine-by-sine basis. Constants R and I are calculated directly from the identification using Eq. (2). Implementation of the dynamic phase compensation controller requires plant identification in a neighborhood of the forcing frequencies. The dynamic compensators H_d and H_x are synthesized from a model fit using the identified plant data and Eqs. (11) and (12). The goal is to create compensator models which diagonalize G_s for all $s < j\omega_x$, where ω_x is some cutoff frequency. The cutoff fre-

Fig. 9 Nyquist plot comparison of static phase compensation (thick solid line) to dynamic phase compensation (thin solid line) for control at $\omega_o = 100$ Hz with measured time constant $\tau = 0.045$ s

quency defines the range, $\omega_o - \omega_x \leq \omega \leq \omega_o + \omega_x$ over which the plant phase will be inverted. A limited range is necessary to synthesize stable, low-order compensator models. The cutoff frequency and model order are chosen for each control loop based on the dynamics of the plant near ω_o. The models are designed to capture large magnitude and phase changes in the empirically generated compensators over the widest frequency range possible while retaining accuracy and stability. Integrators are used in the baseband controller to ensure the Fourier series components of the desired waveform are asymptotically tracked. Additionally, the integrators make the baseband low-pass in nature; therefore, it is more important to capture the dynamics closer to $\omega = 0$.

For example, Fig. 4 displays the empirical and fitted phase compensators used for control at 100 Hz. The diagonal and off-diagonal analytical compensators have been fit up to a frequency of 42 Hz using an eighth and sixth order model, respectively. This lies below the corner frequency of H_{LP} which was set to 50 Hz for these experiments. The model matches the analytical compensators very well at low frequencies and the location of the two modes in each compensator have been captured for both H_d and H_x.

4.4 Test Results. It is fairly commonplace to track or reject sinusoidal references or disturbances at one or two frequencies but for our application the task must be accomplished with a high
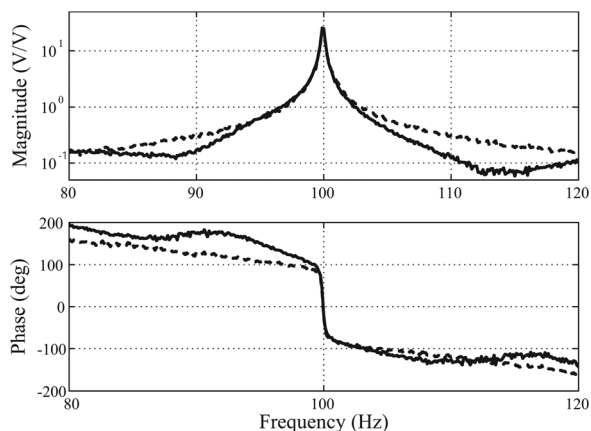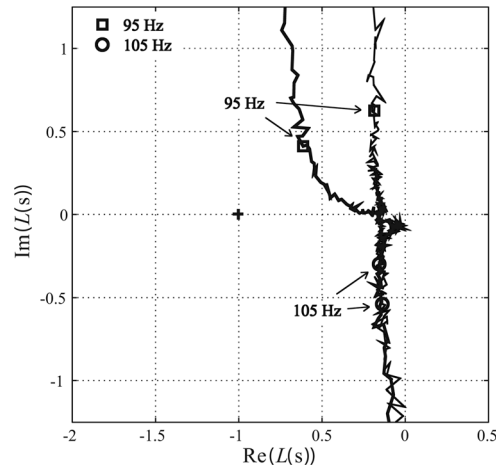

Fig. 8 Loop transfer function comparison of static phase compensation (solid) to dynamic phase compensation (dashed) for control at $\omega_o = 100$ Hz with measured time constant $\tau = 0.045$ s
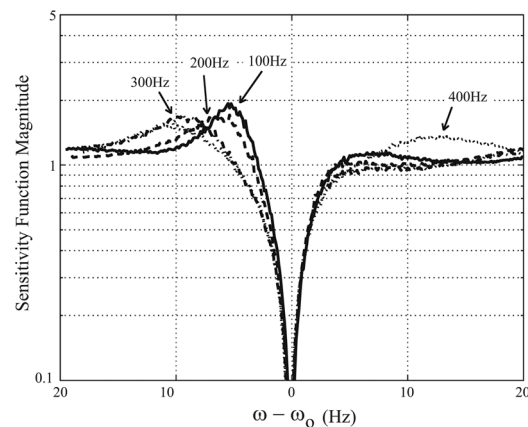

Fig. 10 Sensitivity function comparison of static phase compensation at 100 Hz (solid line), 200 Hz (dashed line), 300 Hz (dot-dashed line), and 400 Hz (dotted line) with measured time constant $\tau = 0.045$ s
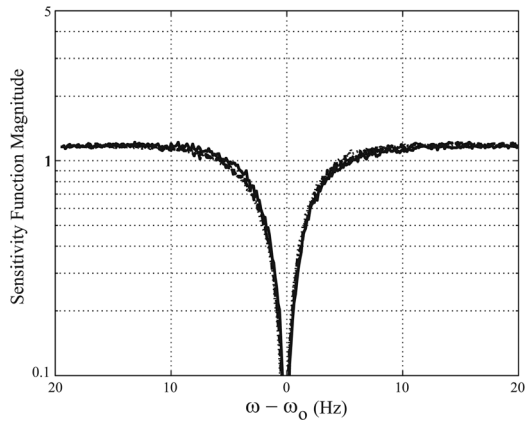
Fig. 11 Sensitivity function comparison of dynamic phase compensation at 100 Hz (solid line), 200 Hz (dashed line), 300 Hz (dot-dashed line), and 400 Hz (dotted line) with measured time constant $\tau = 0.045$ s

number of frequencies in order to form a periodic square wave. In the following experiments we use a 20-frequency modulated-demodulated controller in which dynamic phase compensation was required for [100, 200, 300, 400] Hz. The periodic waveform has a fundamental frequency of 100 Hz. Thus, 20 harmonics fall within the actuation system bandwidth.

The reference signal used for square wave forcing is derived from the Fourier series coefficients of the square wave. The ideal waveform has a frequency defined by the fundamental forcing frequency but has a duty cycle α, the ratio of the temporal pulse width, τ to the waveform period, T, $\alpha = \frac{\tau}{T}$, which is dependent upon user input. The duty cycle is varied to pinpoint the forcing conditions which optimize important characteristics of the jet such as penetration or spread. The desired Fourier series coefficients are tracked using the closed-loop controller to produce waveforms like the two shown with $\alpha = 20\%$ and $\alpha = 40\%$ in Figs. 5(*a*) and 5(*b*), respectively. The measured waveforms in the thin solid line are compared to the ideal square wave in the dashed line and the truncated Fourier series in the thick solid line. In all cases, not just the ones shown here, the measured waveforms match the ideal truncated waveform very well. The small deviations that occur are due

to noise which falls outside the narrow-band regions around each harmonic and, therefore, are uncompensated. Figure 6 shows the measured square wave spectrum and the Fourier series spectrum at each forcing frequency. At these points, the spectra are indistinguishable from one another.

These square waves were formed using a specified closed-loop time constant of $\tau = 0.050$ s, which, using Eq. (7), puts the controller gain at $K = 20/|P(j\omega_o)|$. Figure 7 shows the envelope of the response for a step input with amplitude 1.4 ms^{-1} given only to the 100 Hz control loop. The empirical data are compared to the analytical approximation based on the observation of Eq. (6). The empirical time constant, measured to be $\tau = 0.045$ s, is slightly faster than the specified time constant. As mentioned previously, the convergence rate of the multifrequency controller matches the 100 Hz case presented here because the convergence rates at each frequency of control are equated by adjusting the gain of the individual control loops.

Figure 8 shows a direct comparison of the static and dynamic phase compensation loop gains in the neighborhood of 100 Hz. Both transfer functions move through 0 deg as their phase jumps from 90 deg just below ω_o to −90 deg just after ω_o. However, dynamic phase compensation is shown to reduce the slope of the loop gain phase as compared to the static phase loop transfer function.

A closer look in terms of the stability and sensitivity characteristics of the 100 Hz control loop clearly illustrates the benefit of using dynamic phase compensation over static phase compensation. The Nyquist plot of the 100 Hz static and dynamic phase compensation controller loop gains, L_s and L_d, measured empirically using the $\tau = 0.045$ s controller, is shown in Fig. 9. The locus of L_s moves closer to encircling −1 than L_d at frequencies less than ω_o. This has a significant impact on the phase margin of the controller which is 46.4 deg for static phase compensation but 79.1 deg for dynamic phase compensation.

The improvement in-phase margin from dynamic phase compensation also reduces the maximum sensitivity function magnitude. Figure 10 shows the sensitivity function for 100 Hz as well as 200 Hz, 300 Hz, and 400 Hz using the static phase compensation system with $\tau = 0.045$ s. For comparison, Fig. 11 shows the sensitivity function for dynamic phase compensation at [100, 200, 300, 400] Hz with the same measured time constant, $\tau = 0.045$ s. The 100 Hz static phase sensitivity function has a peak of 1.94 at 94.5 Hz which is reduced beneath 1.2 at all frequencies by
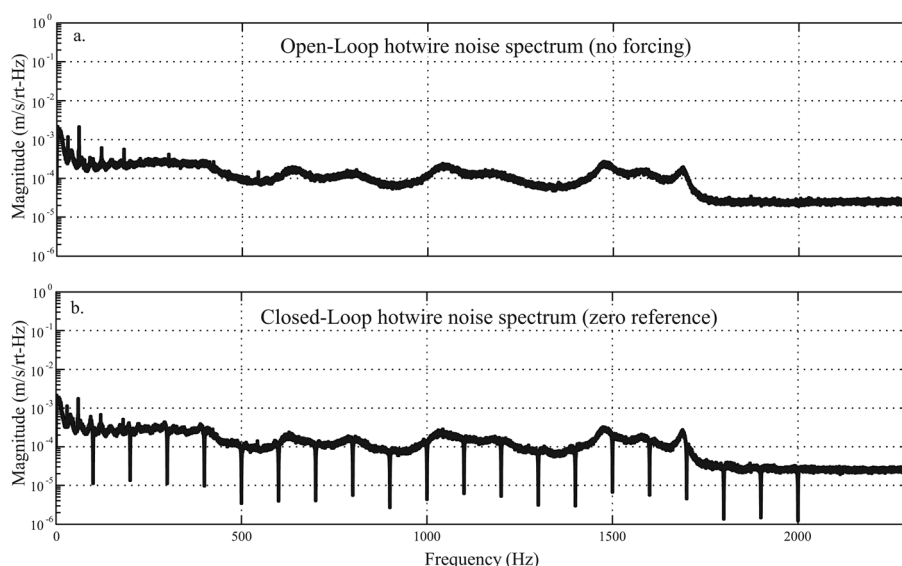

Fig. 12 Hotwire noise spectrum for the open-loop (case a) and closed-loop (case b) system when the reference signal coefficients are zero. Each controller creates a deep notch in the noise spectrum in the closed-loop case. The mean jet velocity is 8 ms^{-1}.
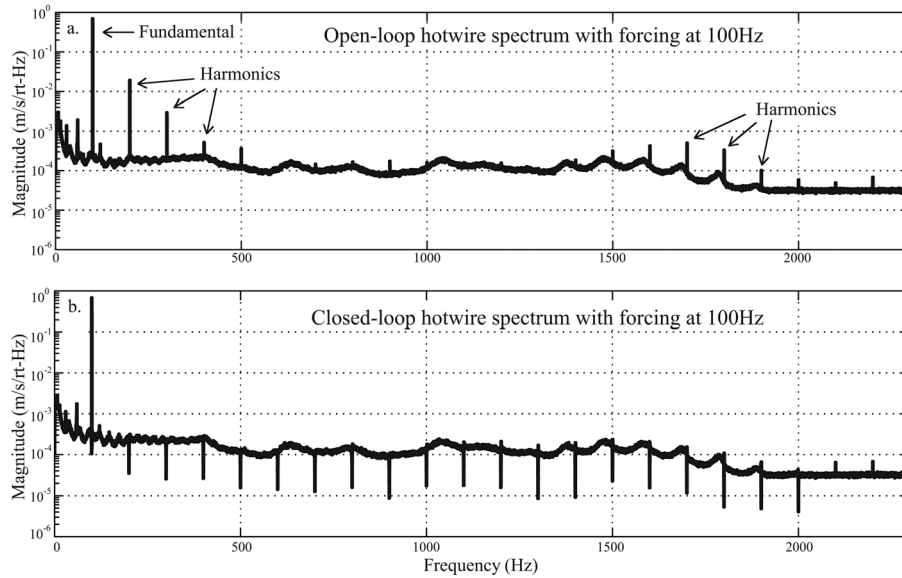
Fig. 13 Suppression of harmonic distortion in response to a 100 Hz single tone input ((*a*) open-loop and (*b*) closed-loop)

dynamic phase compensation. Additionally, the bandwidth of the 100 Hz loop is increased from 6.9 Hz to 10.5 Hz. Between 94.5 Hz and 100 Hz, the plant phase decreases by 36.9 deg, from -95.8 deg to -132.7 deg. The rapidly changing plant phase near ω_o, which can also be seen in the loop transfer function in Fig. 8, is the cause of the peaking in the sensitivity function of the static phase compensation system and makes such an improvement in the dynamic phase compensation system possible. Dynamic phase compensation inverts the plant dynamics at each frequency such that the sensitivity functions at each frequency are almost indistinguishable from one another within the bandwidth of the model fit.

Another demonstration of the multi-frequency modulated-demodulated control approach is presented in Fig. 12, where the effect of closed-loop control on the hotwire noise spectrum is considered. The unforced, open-loop hotwire noise spectrum is shown in Fig. 12(*a*), and the closed-loop hotwire noise spectrum is shown in Fig. 12(*b*). At every frequency of control the closed-loop noise spectrum is reduced well below the broadband noise floor. Although the frequency response data were assumed to have been

generated by a linear plant, there are nonlinear features that can be observed under certain test conditions. For example, the hotwire spectrum exhibits harmonic distortion when the amplifier is driven with a pure tone. The open-loop and closed-loop hotwire spectra are compared again in Fig. 13; however, a single tone at 100 Hz has been imposed which perturbs the mean jet flow by 5%. This example demonstrates the difficulty of forming a square wave through open-loop control because of the excitation of harmonics in response to the forced tone. Perturbations at 200 Hz and many higher frequencies can be seen in the open-loop spectrum of Fig. 13(*a*). These harmonics produce large asymmetries and ringing in the jet's temporal waveform if uncontrolled. The spectrum of the response to the same amplitude input at 100 Hz in Fig. 13(*b*), this time applied with closed-loop control, shows a complete reduction in the harmonic production at all frequencies under control.

Figure 14(*a*) shows the open-loop hotwire spectrum in response to dual tone inputs at 300 Hz and 400 Hz. In addition to harmonics of each tone, subharmonics also appear in the jet response. The production of subharmonics in this manner is similar to
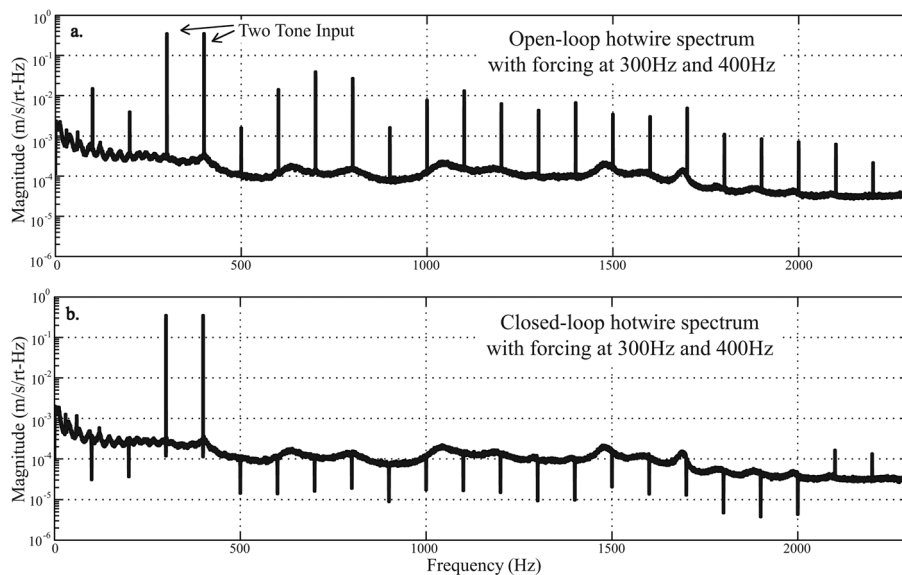

Fig. 14 Elimination of intermodulation distortion in response to a 300 Hz and 400 Hz dual tone input ((*a*) open-loop and (*b*) closed-loop)

intermodulation distortion. Like the 100 Hz single tone case, Fig. 14(*b*) shows closed-loop forcing of these dual tones eliminates the harmonics as well as the subharmonics. At each frequency of control, the spectrum has been reduced significantly beneath the broadband noise floor. Even at harmonics of 300 Hz and 400 Hz above 2000 Hz, the highest frequency of control, the velocity spectrum has been reduced indicating strong coupling between the harmonics.

5 Conclusion

This paper has detailed a useful improvement upon conventional phase compensation of a modulated-demodulated controller and demonstrated an experimental implementation of such a controller for the application of pulsed jet injection via temporal velocity waveform tracking. The use of dynamic phase compensation instead of constant or static phase compensation has reduced peaking in the sensitivity function and increased the bandwidth of systems for control of plants with varying phase near the disturbance or tracking frequency.

It was also shown this controller can be used to simultaneously control a large number of frequencies to track a periodic square wave. The well defined square waves formed in the jet's velocity profile presented in this paper have the potential to significantly improve the spread and mixing of jets used in a variety of aerospace applications.

Acknowledgment

References

[1] Tsao, T. C., and Tomizuka, M., 1994, "Robust Adaptive and Repetitive Digital Tracking Control and Application to a Hydraulic Servo for Noncircular Machining," J. Dyn. Syst. Meas. Control, **116**, pp. 24–32.

[2] Tzou, Y. Y., Ou, R. S., Jung, S. L., and Chang, M. Y., 1997, "High-Performance Programmable ac Power Source With Low Harmonic Distortion Using DSP-Based Repetitive Control Technique," IEEE Trans, Power Electron., **12**, pp. 715–725.

[3] Mattavelli, P., and Ao, F. P. M., 2004, "Repetitive-Based Control for Selective Harmonic Compensation in Active Power Filters," IEEE Trans. Ind. Electron., **51**(5), pp. 1018–1024.

[4] Chew, K. K., and Tomizuka, M., 1990, "Digital Control of Repetitive Errors in Disk Drive Systems," IEEE Control Syst. Mag., **10**, pp. 16–20.

[5] Wu, S.-C., and Tomizuka, M., 2006, "Repeatable Runout Compensation for Hard Disk Drives Using Adaptive Feedforwad Cancellation," *Proceedings of the American Control Conference,* MN, pp. 382–387.

[6] Sacks, A., Bodson, M., and Khosla, P., 1996, "Experimental Results of Adaptive Periodic Disturbance Cancellation in a High Performance Magnetic Disk Drive," ASME J. Dyn. Syst. Meas. Control, **118**, pp. 416–424.

[7] Bittanti, S., and Moiraghi, L., 1994, "Active Control of Vibrations in Helicopters via Pole Assignment Techniques," IEEE Trans. Control Syst. Technol., **2**(4), pp. 343–350.

[8] Ariyur, K. B., and Krstić, M., 1999, "Feedback Attenuation and Adaptive Cancellation of Blade Vortex Interaction on a Helicopter Blade Element," IEEE Trans. Control Syst. Technol., **7**(5), pp. 596–605.

[9] Francis, B. A., and Wonham, W. M., 1975, "The Internal Model Principle for Linear Multivariable Regulators," Appl. Math. Optim., **12**, pp. 457–465.

[10] Kandil, T. H., Khalil, H. K., Vincent, J., Grimm, T. L., Hartung, W., Popielarski, J., York, R. C., and Seshagiri, S., 2005, "Adaptive Feedforward Cancellation of Sinusoidal Disturbances in Superconducting rf Cavities," Nucl. Instrum. Methods Phys. Res., **550**, pp. 514–520.

[11] Byl, M. K., Ludwick, S. J., and Trumper, D. L., 2005, "A Loop Shaping Perspective for Tuning Controllers With Adaptive Feedforward Cancellation," Precis. Eng., **29**, pp. 27–40.

[12] Bodson, M., Sacks, A., and Khosla, P., 1994, "Harmonic Generation in Adaptive Feedforward Cancellation Schemes," IEEE Trans. Autom. Control, **39**, pp. 1939–1944.

[13] Lau, K., Goodwin, G. C., and M'Closkey, R. T., 2005, "Properties of Modulated and Demodulated Systems With Implications to Feedback Limitations," Automatica, **41**, pp. 2123–2129.

[14] Lau, K., Quevedo, D. E., Vautier, B. J. G., Goodwin, G. C., and Moheimani, S. O. R., 2005, "Design of Modultated and Demodulated Controllers for Flexible Structures," Control Eng. Pract., **15**, pp. 377–388.

[15] Goodyear, C. C., 1972, *Signals and Information,* Wiley-Interscience, New York.

[16] Cattell, J., 2003, "Adaptive Feedforward Cancellation Viewed From an Oscillator Amplitude Control Perspective," Master's thesis, Massachusetts Institute of Technology, Cambridge, MA.